

Design of narrow band photonic filter with compact MEMS for tunable resonant wavelength ranging 100 nm

Guanquan Liang, Chengkuo Lee, and Aaron J. Danner

Citation: *AIP Advances* 1, 042171 (2011); doi: 10.1063/1.3670418

View online: <http://dx.doi.org/10.1063/1.3670418>

View Table of Contents: <http://aipadvances.aip.org/resource/1/AAIDBI/v1/i4>

Published by the [American Institute of Physics](#).

Related Articles

Directional waveguide coupling from a wavelength-scale deformed microdisk laser
[Appl. Phys. Lett. 100, 061125 \(2012\)](#)

Tunneling and filtering characteristics of cascaded -negative metamaterial layers sandwiched by double-positive layers
[J. Appl. Phys. 111, 014906 \(2012\)](#)

Measurement of phase retardation of waveplate online based on laser feedback
[Rev. Sci. Instrum. 83, 013101 \(2012\)](#)

Simple alignment technique for polarisation maintaining fibres
[Rev. Sci. Instrum. 82, 125103 \(2011\)](#)

Polarization dependent state to polarization independent state change in THz metamaterials
[Appl. Phys. Lett. 99, 221102 \(2011\)](#)

Additional information on AIP Advances

Journal Homepage: <http://aipadvances.aip.org>

Journal Information: <http://aipadvances.aip.org/about/journal>

Top downloads: http://aipadvances.aip.org/most_downloaded

Information for Authors: <http://aipadvances.aip.org/authors>

ADVERTISEMENT

NEW!

iPeerReview
AIP's Newest App



**Authors...
Reviewers...
Check the status of
submitted papers remotely!**

AIP | Publishing

Design of narrow band photonic filter with compact MEMS for tunable resonant wavelength ranging 100 nm

Guanquan Liang,^a Chengkuo Lee, and Aaron J. Danner

Department of Electrical and Computer Engineering, National University of Singapore, Singapore 117576, Singapore

(Received 3 August 2011; accepted 21 November 2011; published online 9 December 2011)

A prototype of planar silicon photonic structure is designed and simulated to provide narrow resonant line-width (~ 2 nm) in a wide photonic band gap (~ 210 nm) with broad tunable resonant wavelength range (~ 100 nm) around the optical communication wavelength 1550 nm. This prototype is based on the combination of two modified basic photonic structures, i.e. a split tapered photonic crystal micro-cavity embedded in a photonic wire waveguide, and a slot waveguide with narrowed slabs. This prototype is then further integrated with a MEMS (microelectromechanical systems) based electrostatic comb actuator to achieve “coarse tune” and “fine tune” at the same time for wide range and narrow-band filtering and modulating. It also provides a wide range tunability to achieve the designed resonance even fabrication imperfection occurs. *Copyright 2011 Author(s). This article is distributed under a Creative Commons Attribution 3.0 Unported License.* [doi:10.1063/1.3670418]

To form a narrow band tunable filter based on photonic crystals, a nano cavity is usually introduced in-between periodic structures to generate a narrow resonant peak inside the photonic band gap.¹ To tune the resonant wavelength, usually a refractive index change by carrier injection is applied to the cavity region.²⁻⁴ However, the change available from this effect is only approximately of order 10^{-2} to 10^{-3} and thus can provide only ~ 5 nm tunability. Micro-electromechanical systems (MEMS) induced effective index change also provides similar results.⁵ As improvement, there are experimental demonstrations of electrostatically tunable photonic crystal cavities that provide 10 nm and 20 nm tuning range for narrow band resonance.^{6,7} In order to have a widely tunable filter with tuning range ~ 100 nm, some optical designs have been shown, including a distributed Bragg reflector in a liquid crystal waveguide⁸ with a large footprint size of 1.5 mm and a birefringent hollow waveguide⁹ with a wide signal band. Hence, a small footprint optical filter that is compatible with integrated silicon nano photonics and provides narrow band filtering with a wide tunable range (e.g., up to 100 nm) will be a further advance in this area.

In this work, we propose such a tunable silicon photonic structure integrated with a compact electrostatic MEMS comb actuator. Through 45 nm continuous and smooth displacement of the tunable photonic structure by MEMS electrostatic actuation, a narrow resonant peak ~ 2 nm of full width at half maximum (FWHM) can be shift in a range of 100 nm around 1550 nm for optical communication and at the same time keeps a wide photonic bandgap (~ 210 nm) invariant through the whole tuning process.

First, we focus on the design of the optical component. We begin with a tapered photonic nano cavity embedded in a Si (refractive index $n=3.48$) photonic wire, as shown in Fig. 1(a). It is suspended in air, which can be fabricated by electron-beam lithography on a silicon-on-insulator (SOI) wafer followed by reactive ion etching and HF wet etching with standard procedures.¹⁰ This kind of basic structure provides a resonant peak within the photonic band gap. The band gap width is determined by the filling fraction and the center-to-center distance between the neighboring holes

^aCorresponding author: elegq@nus.edu.sg



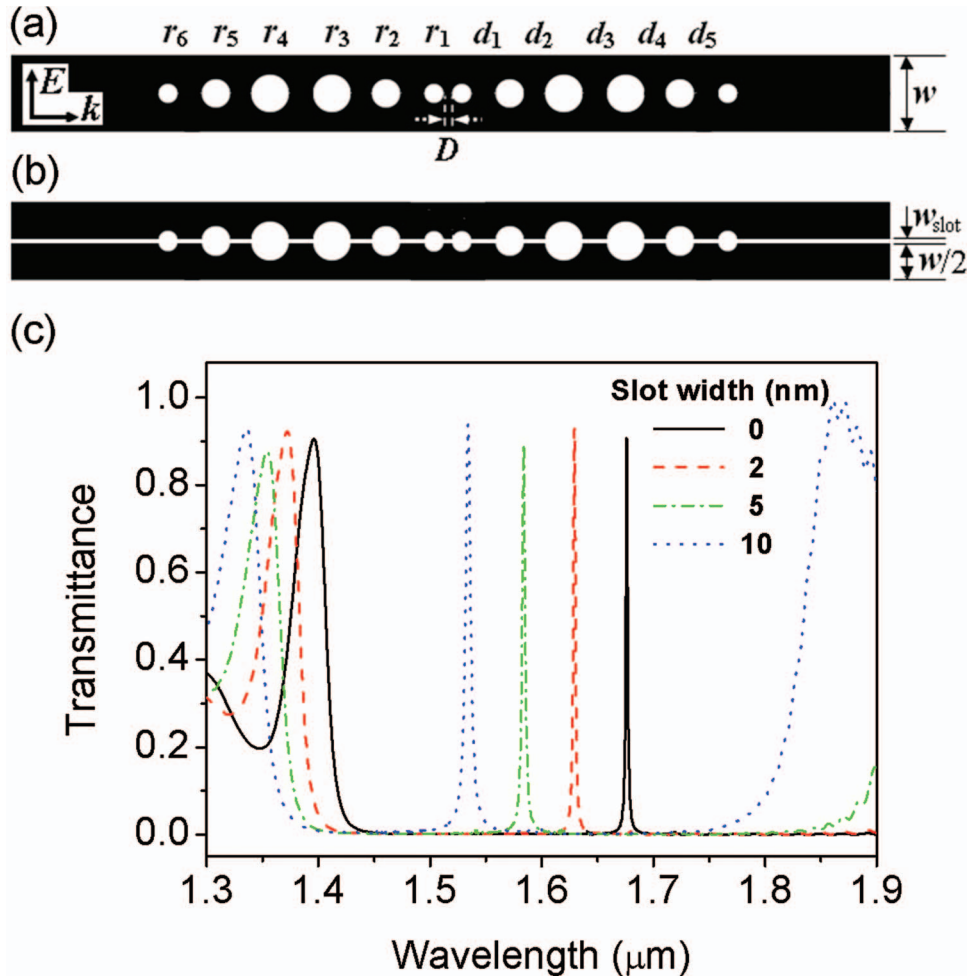


FIG. 1. Tapered photonic cavity in silicon photonic wire with (a) and without (b) air slot. (c) Transmission spectra of TM-polarization as defined in (a) showing narrow resonance tunable over ~ 150 nm in wavelength from 2D simulation by only changing the slot width w_{slot} from 0 nm to 10 nm.

(d_i , $i=1,2,3, \dots$). The filling fraction is determined by the radii of the air holes (r_i) and the width of the photonic wire (w). The position of the resonant peak relative to the band gap is determined by the length of the defect (D). The thickness of the photonic wire is t . For a filter, relatively high contrast between the transmission of the resonant peak and the band gap should also be considered.

Simulations were performed with the finite-difference time-domain (FDTD) method,¹¹ using a freely available software package.¹² Using TM-polarization as defined in Fig. 1(a), the solid curve in Fig. 1(c) shows the transmission of the structure in Fig. 1(a) by a 2D simulation (3D simulations will follow this basic design discussion), where $w=500$ nm, $r_1=r_6=60$ nm, $r_2=r_5=90$ nm, $r_3=r_4=120$ nm, $d_1=d_5=310$ nm, $d_2=d_4=350$ nm, $d_3=400$ nm, and $D=60$ nm. It shows a narrow resonant peak within a wide photonic band gap. Then for tuning the resonant wavelength by introducing effective index change and providing MEMS tunability, in Fig. 1(b), we symmetrically divided the tapered waveguide into two equal separated strips throughout its length and introduce an air slot with width w_{slot} . The dotted curve in Fig. 1(c) shows that even a 10 nm slot can blue-shift the resonant wavelength by ~ 150 nm. At the same time, the band gap is narrowed and blue shifts. The slot width can be controlled, e.g. by attaching the strips to electrostatic MEMS comb actuator.⁵

Such a sensitive design may only be practical if smooth sidewalls with roughness less than 1 nm are achievable, so we instead intend to have a practical design with slot width of tens of nanometers. However, a wide air slot significantly reduces local refractive index contrast between regions with

and without the air holes; consequently it shrinks the band gap width a lot to the point of being useless. The radii of the holes should therefore be enlarged to keep enough effective index contrast to open up a relatively wide band gap. However, having enlarged radii means a reduction of silicon area which is used to guide light by index confinement, and an increase of scattering probability, especially in the out of plane direction. Notice that the result in Fig.1(c) is from a 2D simulation. It can be imagined that when a finite thickness, e.g. $t = 500$ nm (a typical value in SOI based photonic device design), is applied to the waveguide, most energy of the resonant mode will be scattered away, and its transmission will be dramatically reduced.

In order to obtain relatively high transmission for this split tapered waveguide with finite thickness, a slot waveguide is utilized. This is because a slot waveguide transmits TM-polarized light through its nano slot by index-discontinuity with high transmission.¹³⁻¹⁵ Here, we modify the width of each slab (w_{slab}) of the slot waveguide to be tens of nm, and then merge such slabs into the split tapered photonic nano cavity, as shown in Fig. 2(a), which presents the prototype of the tunable photonic structure proposed. The split photonic nano cavity (in red) is partially covered by the modified slot waveguide (in blue, starting from the edges of the air slot).

3D simulation for the transmission of this design is then carried out. Fig.2(b) compares the transmission from the structures with various widths of the slab w_{slab} , and all the other structural parameters are the same at $t=500$ nm, $w_{\text{slot}}=40$ nm, $w/2=250$ nm, $r_1=r_8=110$ nm, $r_2=r_7=140$ nm, $r_3=r_6=180$ nm, $r_4=r_5=210$ nm, $d_1=240$ nm, $d_2=390$ nm, $d_3=d_5=540$ nm, $d_4=600$ nm, $d_6=d_7=450$ nm, and $D=140$ nm. Fig.2(b) shows that a proper width of the slab can largely increase the transmission by ~ 100 times compared to the structure without the modified slot waveguide; also the wider w_{slab} , the higher the transmittance and the wider the FWHM of the resonant peak, while the narrower the photonic bandgap. $w_{\text{slab}}=75$ nm provides a good trade-off for transmission $\sim 75\%$, FWHM ~ 2 nm and bandgap width ~ 350 nm, which will be used in Fig.3 and 4. The transmission in 3D simulation is normalized to a silicon rib with the same thickness surrounding by air; and in 2D is normalized to a silicon rib with infinite height.

Fig.3(a) shows that within a photonic band gap (from 1460 nm to 1670 nm), the resonant wavelength can be continuously tuned by ~ 100 nm (from 1622 nm to 1524 nm) when the width of the air slot is continuously changed from 35 nm to 80 nm. Fig.3(b) and its inset show the FWHM ranges of the resonant peaks as a function of the slot width. Fig.3(a) and 3(b) indicate that throughout the whole tuning range, the resonant peak will be as narrow as ~ 2 nm with transmission $\sim 70\%$. Here we just demonstrate an example of this in simulation. The FWHM can be further narrowed by increasing the number of air holes, and the transmission can also be further increased by optimizing the radii of the holes and distances between them. The typical electric field distribution of the resonant mode, e.g. when $w_{\text{slot}}=60$ nm, is shown in Fig.3(c) for both the top view and the side view. They show that most energy of the resonant mode is strongly localized in the central slot to be transmitted, and its quality factor is 783 as calculated with MEEP.

In our design, the air holes change their shapes from half circles to be less than half circles, providing enough refractive index contrast by their relatively large radii to generate a relatively large band gap. The shape and orientation of the air holes make the split structure be a united one, as can be seen from the field distribution in Fig.3(c), instead of two coupled nano cavities. The coupling of two nano cavities would provide two resonant peaks^{5,16} while our design offers a single tunable resonant peak throughout the whole tuning range, as shown in Fig.3. The nano air slot sandwiched by parallel slabs reduces light scattering from the openings of half circles and provides index-discontinuity guiding of light to achieve high transmission. For other thicknesses of the device layer in an SOI system, the same design method can be applied.

The above optical design is then attached to a designed comb-drive electrostatic MEMS for tuning the slot width, as shown in Fig.4(a), where only half of the structure is simulated with $X=0$ as a mirror plane. The photonic filter is located from $Y=0$ to $Y=535$ nm with original air slot width 35 nm. The MEMS structure is located from $Y=535$ nm to $Y=3.5 \mu\text{m}$ (fixed boundary). The whole volume of the device is as compact as $10 \mu\text{m}$ long, $3.5 \mu\text{m}$ wide and 500 nm high. 3D finite element analysis¹⁷ with Young's modulus (170 GPa) and Poisson's ratio (0.28) of crystalline silicon is used to simulate the MEMS actuation. The displacements of the center ($X=0$) and the end ($X=5 \mu\text{m}$) of the strip are shown in Fig.4(b). Their difference is less than 0.2 nm, so the upper strip of the photonic

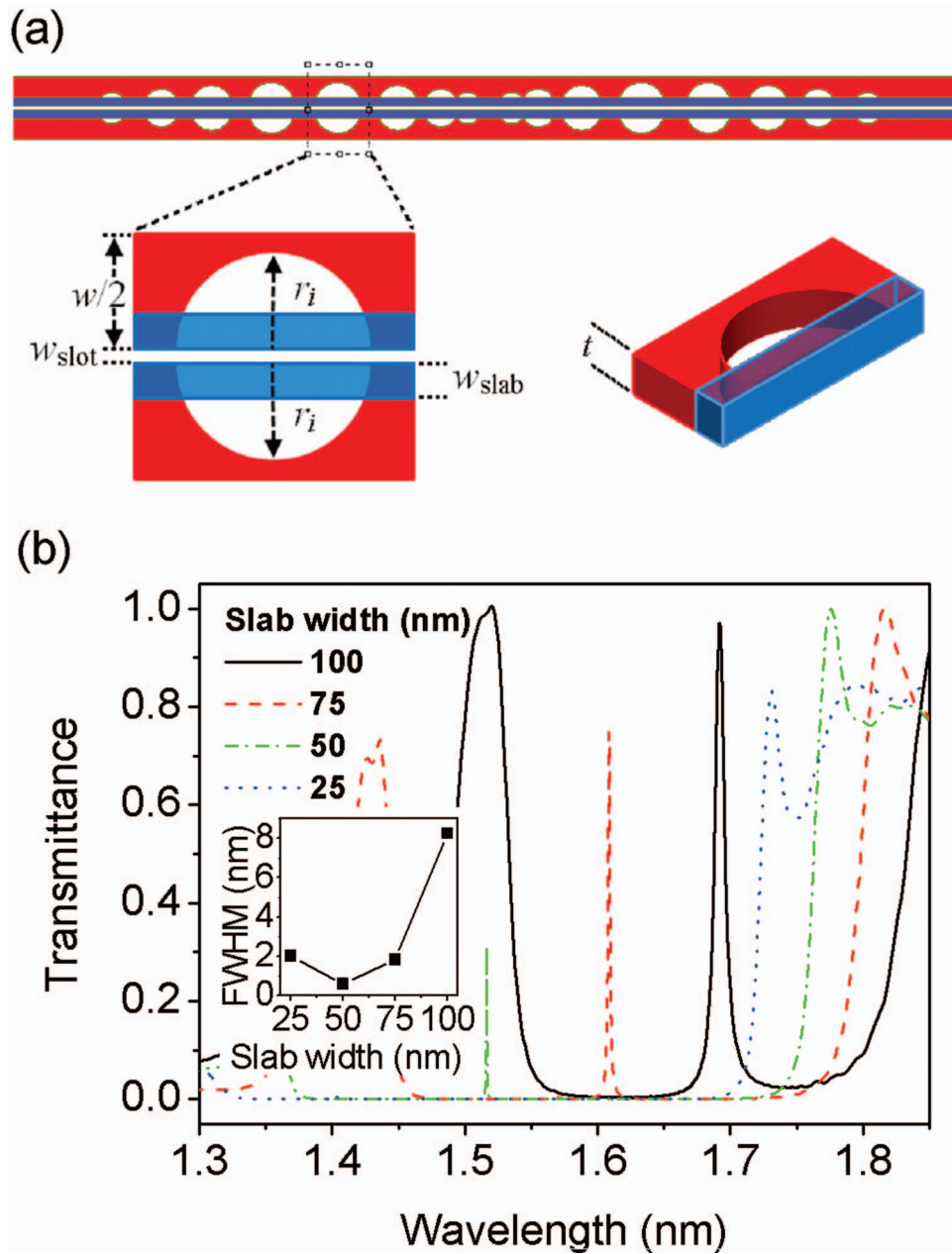


FIG. 2. (a) Split tapered photonic cavity in silicon photonic wire (in red) merged with nano air slot waveguide with narrowed slabs (in blue). (b) Transmission spectra from 3D simulation compares the FWHM of the resonant peaks (see also the inset) and the width of corresponding photonic bandgaps, as a function of the slab width w_{slab} from 25 nm to 100 nm.

filter can be shifted upward with its edge kept parallel to the lower strip, as shown in Fig.4(a), which is consistent with the working principle of the photonic filter designed. The displacement of the strip is equivalent to an increase of the air slot width in the photonic filter. From Fig.3(a), the maximum increase of the air slot width needed is only 45 nm, so from Fig.4(b) the actuation voltage range used will be from 0 to 67.5 V, and both coarse and fine tuning can be realized by this compact MEMS design for compensating nano fabrication errors. Inset of Fig.4(b) shows resonant wavelength tuning vs. actuation voltage, as determined from Fig.3(b) and 4(b). The resonant wavelength of the narrow band filter can be tuned in a range of ~ 100 nm when the actuation voltage is applied from 0 to 67.5 V. For non-degraded optical performance with MEMS connection, we found that the distance between

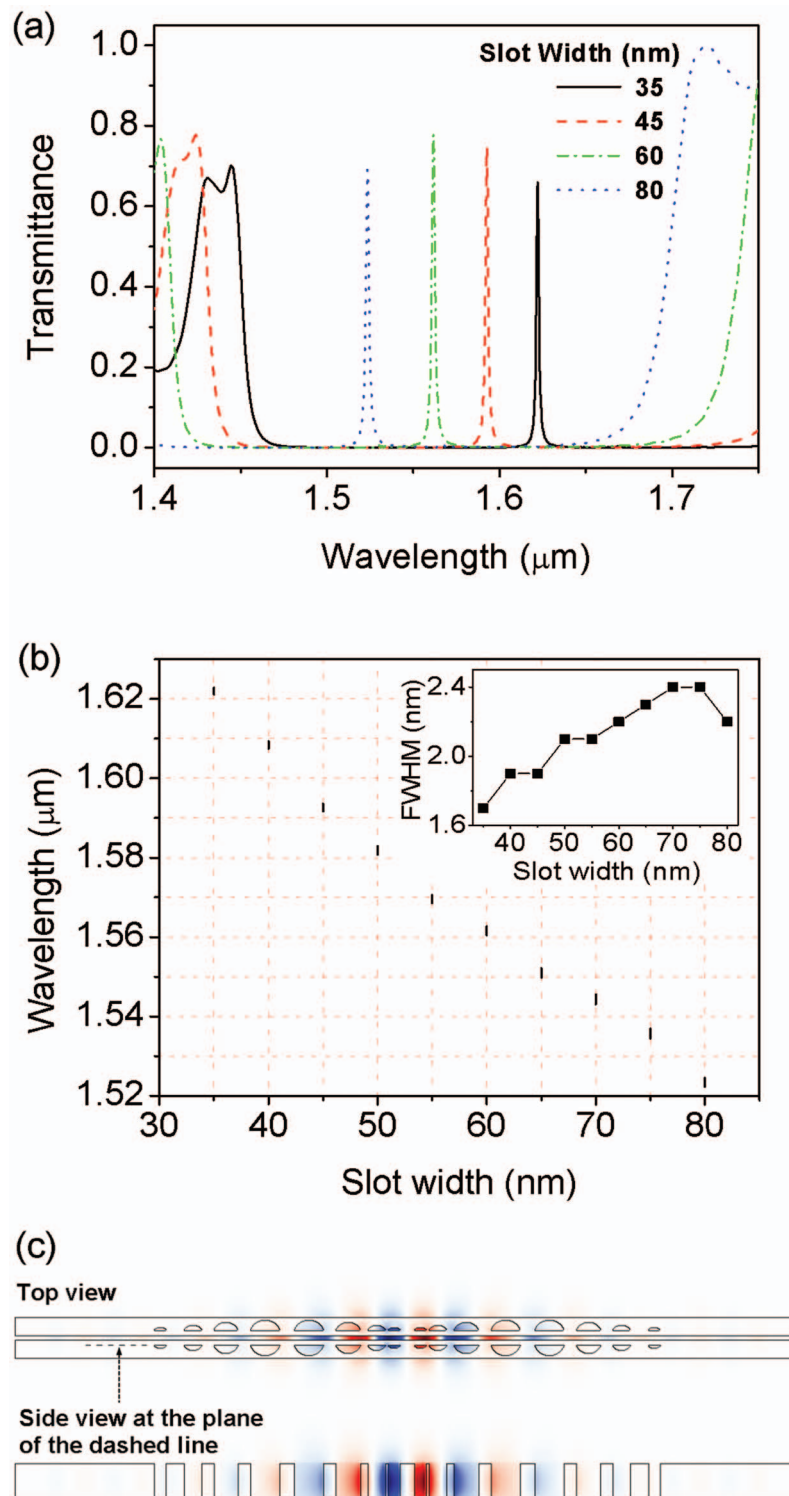


FIG. 3. (a) Transmission spectra from 3D simulation of the designed structure and (b) FWHM ranges (inset: FWHM) of the resonant peaks as a function of the air slot width w_{slot} when the slab width $w_{\text{slab}}=75$ nm. (c) A typical electric field distribution of the resonant peak, taking $w_{\text{slot}}=60$ nm as an example.

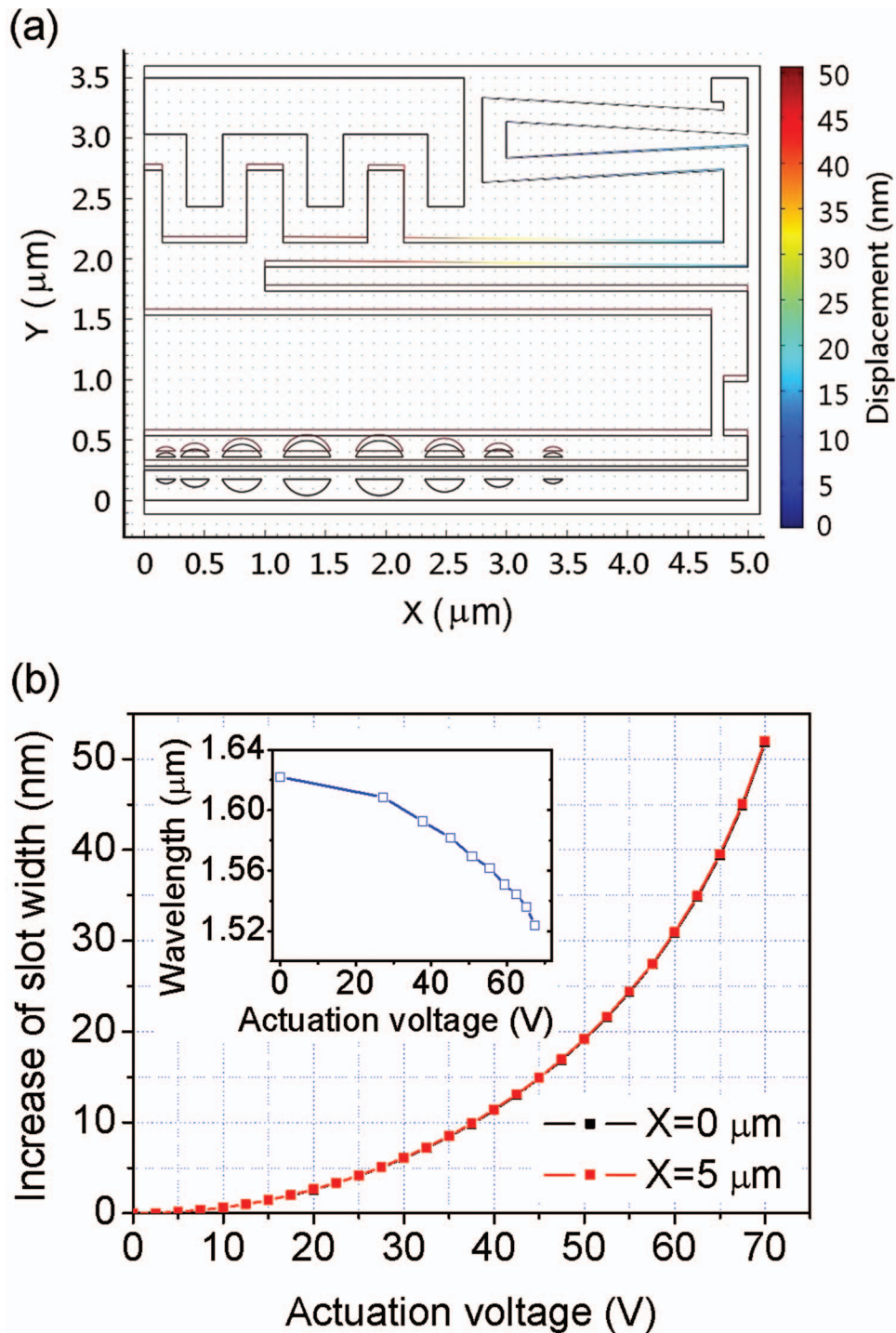


FIG. 4. (a) Designed comb drive MEMS actuating the designed tunable photonic filter to change the air slot width. Color bar shows the value of displacement. (b) Displacements of the center ($X=0 \mu\text{m}$) and the end ($X=5 \mu\text{m}$) of the upper strip of the photonic filter as a function of the actuation voltage between the combs in the MEMS. Inset: resonant wavelength tuning vs. actuation voltage, as determined from Fig.3(b) and 4(b).

the photonic filter and the MEMS main body should be at least $1\ \mu\text{m}$, and the connection between them should be at least $1\ \mu\text{m}$ away from the holes of the photonic filter, as shown in Fig.4(a).

In conclusion, based on the combination of two modified basic photonic structures, i.e. a split tapered photonic crystal micro-cavity embedded in a photonic wire waveguide, and a slot waveguide with narrowed slabs, a kind of planar silicon photonic structure is designed and simulated to provide a narrow resonant line-width ($\sim 2\ \text{nm}$) in a wide photonic band gap ($\sim 210\ \text{nm}$) with a very broad tunable resonant wavelength range ($\sim 100\ \text{nm}$) around the optical communication wavelength $1550\ \text{nm}$. A compact electrostatic MEMS comb actuator is also designed to achieve coarse and fine tuning of the optical filter at the same time for wide range and narrow-band filtering and modulating. This MEMS driven widely tunable narrow band optical filter also provides a solution to bring the actual resonant wavelength to be the designed one if any fabrication error occurs; even the difference between them is as large as $100\ \text{nm}$.

ACKNOWLEDGMENTS

This work was supported in part by Singapore's A*Star Science and Engineering Research Council (SERC) grant 0921010049.

- ¹J. S. Foresi, P. R. Villeneuve, J. Ferrera, E. R. Thoen, G. Steinmeyer, S. Fan, J. D. Joannopoulos, L. C. Kimerling, H. I. Smith, and E. P. Ippen, *Nature* **390**, 143 (1997).
- ²M. Y. Liu and S. Y. Chou, *Appl. Phys. Lett.* **68**, 170 (1996).
- ³B. Schmidt, Q. Xu, J. Shakya, S. Manipatruni, and M. Lipson, *Opt. Express* **15**, 3140 (2007).
- ⁴M. Xin, A. J. Danner, C. E. Png, and S. T. Lim, *J. Opt. Soc. Am. B* **26**, 2176 (2009).
- ⁵X Chew, G Zhou, F S Chau, J Deng, X Tang, and Y C Loke, *Opt. Express* **18**, 22232 (2010).
- ⁶I. W. Frank, P. B. Deotare, M. W. McCutcheon, and M. Loncar, *Optics Express*, **18**, 8705 (2010).
- ⁷R. Perahia, J. D. Cohen, S. Meenehan, T. P. Mayer Alegre, and O. Painter, *Appl. Phys. Lett.*, **97**, 191112 (2010).
- ⁸G. Gilardi, R. Asquini, A. d'Alessandro, and G. Assanto, *Opt. Express* **18**, 11524 (2010).
- ⁹M. Kumar, T. Sakaguchi, and F. Koyama, *Opt. Lett.* **34**, 1252 (2009).
- ¹⁰A. R. Md Zain, N. P. Johnson, M. Sorel, and R. M. De La Rue, *IEEE Photon. Technol. Lett.* **21**, 1789 (2009).
- ¹¹A. Taflove and Susan C. Hagness, *Computational Electrodynamics: The Finite-Difference Time-Domain Method* (Artech: Norwood, MA, 2000).
- ¹²A. F. Oskooi, D. Roundy, M. Ibanescu, P. Bermel, J. D. Joannopoulos, and S. G. Johnson, *Computer Physics Communications* **181**, 687 (2010).
- ¹³V. R. Almeida, Q. Xu, C. A. Barrios, and M. Lipson, *Opt. Lett.* **29**, 1209 (2004).
- ¹⁴Q. Xu, V. R. Almeida, R. R. Panepucci, and M. Lipson, *Opt. Lett.* **29**, 1626 (2004).
- ¹⁵J. T. Robinson, C. Manolatu, L. Chen, and M. Lipson, *Phys. Rev. Lett.* **95**, 143901 (2005).
- ¹⁶P. B. Deotare, M. W. McCutcheon, I. W. Frank, M. Khan, and M. Loncar, *Appl. Phys. Lett.* **95**, 031102 (2009).
- ¹⁷COMSOL Multiphysics, <http://www.comsol.com>.